KU LEUVEN

FACULTEIT
INGENIEURSWETENSCHAPPEN

B-KUL-H04X3A: Control Theory

Team members:

Lefebure Tiebert (r0887630)
Campaert Lukas (r0885501)

Assignment 1: Identification of the Cart

Professor:

Prof. Dr. Ir. Jan Swevers

Academic Year 2025-2026

Declaration of Originality

We hereby declare that this submitted draft is entirely our own, subject to feedback and support given us by the didactic team, and subject to lawful cooperation which was agreed with the same didactic team. Regarding this draft, we also declare that:

1. *Note has been taken of the text on academic integrity* `https://eng.kuleuven.be/studeren/masterproef-en-papers/documenten/20161221-academischeintegriteit-okt2016.pdf`.
2. *No plagiarism has been committed as described on* `https://eng.kuleuven.be/studeren/masterproef-en-papers/plagiaat#Definitie:%20wat%20is%20plagiaat?`.
3. *All experiments, tests, measurements, …, have been performed as described in this draft, and no data or measurement results have been manipulated.*
4. *All sources employed in this draft – including internet sources – have been correctly referenced.*

1 Discrete-time model structure selection

We assume that (i) the same voltage is applied to both motors, (ii) no wheel slip occurs, (iii) only longitudinal motion (no turning) is considered, and (iv) the cart mass and ground friction are lumped into the wheel inertia and viscous friction, respectively. Under these assumptions, the lumped-parameter model follows from the balance of angular momentum of the rotor and the conservation of electric charge in the armature circuit.

Taking the Laplace transform of these equations (see Figure 4 in Appendix B) and solving for $\dot{\Theta}_m(s)/V_a(s)$ yields the following transfer function:

$$H(s) = \frac{\dot{\Theta}_m(s)}{V_a(s)} = \frac{K}{\big(J_m s + b\big)\big(L_a s + R_a\big) + K^2} \tag{1}$$

Symbol	Description
$\dot{\Theta}_m(s)$	Laplace transform of the angular velocity $\dot{\theta}_m$ [rad/s]
$V_a(s)$	Laplace transform of the applied voltage v_a [V]
J_m	moment of inertia of the rotor [kg m^2]
b	damping coefficient (viscous friction) [N m s/rad]
K	motor torque and back EMF constant [N m/A] or [V s/rad]
L_a	armature inductance [H]
R_a	armature resistance [Ω]

This continuous-time transfer function relates the input voltage $v_a(t)$ to the rotational speed of the motor shaft $\dot{\theta}_m(t)$. We can represent the transfer function with generic coefficients since the exact values of the physical constants are unknown and will be estimated later. Therefore, $H(s)$ becomes:

$$H(s) = \frac{\dot{\Theta}_m(s)}{V_a(s)} = \frac{a}{bs^2 + cs + d} \tag{2}$$

1.1 Discrete-time transfer function

The discrete-time transfer function with computational delay is:

$$H(z) = \frac{b_1 z + b_2}{z^3 + a_1 z^2 + a_2 z} \tag{3}$$

This is a third-order model with numerator order 1, denominator order 3, and relative order 2 (indicating two delays: one from motor dynamics and one from microOS latency).

1.2 Model derivation

To obtain a discrete-time model, the continuous-time system

$$H(s) = \frac{a}{bs^2 + cs + d}$$

is sampled with sampling period T_s under a zero-order hold (ZOH) on the input. The ZOH assumption implies that the input voltage is piecewise constant on each sampling interval $[kT_s, (k+1)T_s)$. For a strictly proper second-order transfer function, ZOH discretization yields a second-order discrete-time transfer function

$$H_0(z) = \frac{b_1 z + b_0}{z^2 + a_1 z + a_0}, \tag{4}$$

with coefficients a_0, a_1, b_0, b_1 that follow from the sampled state-space dynamics

$$x((k+1)T_s) = e^{AT_s} x(kT_s) + \int_0^{T_s} e^{A\tau} B \, d\tau \, u(kT_s),$$

with $y(kT_s) = Cx(kT_s)$, and then forming the corresponding transfer function.

The computational latency of the microOS introduces an additional one-sample delay between the computed control signal and the applied motor voltage. In the z-domain this corresponds to a multiplicative factor z^{-1}, so the overall discrete-time transfer function becomes

$$H(z) = z^{-1}H_0(z) = \frac{b_1 z + b_2}{z^3 + a_1 z^2 + a_2 z}, \tag{5}$$

During identification these four parameters are estimated directly from the measured input-output data, so no explicit mapping back to the continuous-time coefficients is required.

1.3 Model structure motivation

We consider two candidate model structures: (i) the full third-order model above, which accounts for armature inductance, and (ii) a reduced second-order model obtained by neglecting the armature inductance L_a, leading to

$$H(z) = \frac{b_1}{z^2 + a_1 z},$$

with only two parameters.

2 Model parameters estimation

We estimate the parameters of the third-order discrete-time transfer function $H(z) = \frac{b_1 z + b_2}{z^3 + a_1 z^2 + a_2 z}$ using linear least squares. The matrix formulation of the parameter estimation problem of the second-order model is presented in Appendix A.

2.1 Recursion expression and error criterion

The difference equation for the third-order model is:

$$\dot{\theta}[k] = -a_1\dot{\theta}[k-1] - a_2\dot{\theta}[k-2] + b_1 v[k-2] + b_2 v[k-3] \tag{6}$$

This can be written in compact form as $\dot{\theta}[k] = \boldsymbol{\theta}^T \boldsymbol{\phi}[k]$ with parameter vector and regression vector:

$$\boldsymbol{\theta} = \begin{bmatrix} a_1 \\ a_2 \\ b_1 \\ b_2 \end{bmatrix}, \quad \boldsymbol{\phi}[k] = \begin{bmatrix} -\dot{\theta}[k-1] \\ -\dot{\theta}[k-2] \\ v[k-2] \\ v[k-3] \end{bmatrix} \tag{7}$$

For the simplified second-order model, the recursion reduces to:

$$\dot{\theta}[k] = -a_1\dot{\theta}[k-1] + b_1 v[k-2] \tag{8}$$

with corresponding parameter and regression vectors

$$\boldsymbol{\theta}_{\text{simp}} = \begin{bmatrix} a_1 \\ b_1 \end{bmatrix}, \quad \boldsymbol{\phi}_{\text{simp}}[k] = \begin{bmatrix} -\dot{\theta}[k-1] \\ v[k-2] \end{bmatrix}. \tag{9}$$

The least squares criterion minimizes the sum of squared prediction errors:

$$V_N(\boldsymbol{\theta}) = \sum_{k=1}^{N} \frac{1}{2}[\dot{\theta}[k] - \boldsymbol{\phi}^T[k]\boldsymbol{\theta}]^2 \tag{10}$$

2.2 Matrix formulation

For N measurements with maximum delay of 3 samples, the output vector (starting from $k = 4$) and regression matrix are:

$$\boldsymbol{y} = \begin{bmatrix} \dot{\theta}[4] \\ \dot{\theta}[5] \\ \vdots \\ \dot{\theta}[N] \end{bmatrix}, \quad \boldsymbol{\Phi} = \begin{bmatrix} -\dot{\theta}[3] & -\dot{\theta}[2] & v[2] & v[1] \\ -\dot{\theta}[4] & -\dot{\theta}[3] & v[3] & v[2] \\ \vdots & \vdots & \vdots & \vdots \\ -\dot{\theta}[N-1] & -\dot{\theta}[N-2] & v[N-2] & v[N-3] \end{bmatrix} \tag{11}$$

The least squares solution is:

$$\hat{\boldsymbol{\theta}}_N^{LS} = [\boldsymbol{\Phi}^T \boldsymbol{\Phi}]^{-1} \boldsymbol{\Phi}^T \boldsymbol{y} = \boldsymbol{\Phi}^+ \boldsymbol{y} \tag{12}$$

where $\boldsymbol{\Phi}^+$ is the Moore-Penrose pseudo-inverse.

3 Identification of the cart by exciting the motors while the cart is on the ground

3.1 Excitation signal selection

3.1.1 Motivation for excitation signal

A periodic piecewise-constant multilevel excitation signal is used for system identification. Such signals are persistently exciting, cover multiple operating points, and generate sufficiently rich frequency content for reliable parameter estimation. The input alternates between four nonzero voltage levels (+6 V +5 V −6 V −5 V) and zero-voltage plateaus so that both transient and steady-state responses are observable. The use of multiple amplitudes facilitates verification of approximate linearity, guarantees input levels high enough to overcome static friction and excites the dominant modes of the motor-cart dynamics.

3.1.2 Excitation signal design and implementation

The excitation has a period of 14 s with the sequence

+6 V (0–2 s), 0 V (2–3 s), +5 V (3–5 s), 0 V (5–7 s), −6 V (7–9 s), 0 V (9–10 s), −5 V (10–12 s), 0 V (12–14 s).

The signal is sampled at $f_s = 100$ Hz and applied for two full periods (total duration 28 s), as shown in Figure 1. Repetition of the cycle increases the effective SNR via averaging over periods, yields a data record of sufficient length for parameter estimation and permits an empirical assessment of measurement noise by comparing responses to identical input segments.

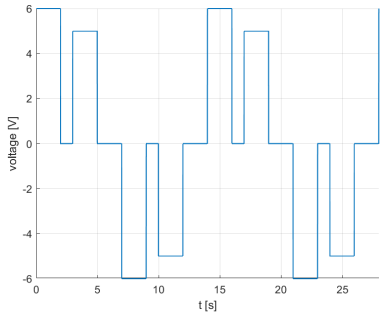

Figure 1: Applied excitation signal over 2 complete periods (28 seconds)

3.2 Parameter estimation and model validation for both motors

Using linear least squares estimation, we identified both the third-order model ($H(z) = \frac{b_1 z + b_2}{z^3 + a_1 z^2 + a_2 z}$) and the simplified second-order model ($H(z) = \frac{b_1}{z^2 + a_1 z}$) for motors A and B.
The simplified-model parameter vectors, identified on the unfiltered data set with sampling time $T_s = 0.01$ s, are

$$\hat{\boldsymbol{\theta}}_A^{\text{simp}} = \begin{bmatrix} -0.6819 \\ 0.6309 \end{bmatrix}, \qquad \hat{\boldsymbol{\theta}}_B^{\text{simp}} = \begin{bmatrix} -0.6806 \\ 0.6488 \end{bmatrix}. \tag{13}$$

The resulting discrete-time transfer functions are

$$\hat{H}_A^{\text{simp}}(z) = \frac{0.6309}{z^2 - 0.6819z}, \qquad \hat{H}_B^{\text{simp}}(z) = \frac{0.6488}{z^2 - 0.6806z}. \tag{14}$$

The full model estimated parameter vectors are

$$\hat{\boldsymbol{\theta}}_A = \begin{bmatrix} -0.5671 \\ -0.0970 \\ 0.0077 \\ 0.6589 \end{bmatrix}, \quad \hat{\boldsymbol{\theta}}_B = \begin{bmatrix} -0.5762 \\ -0.0881 \\ 0.0081 \\ 0.6741 \end{bmatrix}. \tag{15}$$

The corresponding discrete-time transfer functions without the explicit one-sample delay are

$$\hat{H}_{0,A}(z) = \frac{0.007672z + 0.6589}{z^2 - 0.5671z - 0.09698}, \tag{16}$$

$$\hat{H}_{0,B}(z) = \frac{0.008073z + 0.6741}{z^2 - 0.5762z - 0.08815}. \tag{17}$$

Including the microOS delay yields the third-order models reported throughout this section:

$$\hat{H}_A(z) = z^{-1}\hat{H}_{0,A}(z) = \frac{0.007672z + 0.6589}{z^3 - 0.5671z^2 - 0.09698z}, \tag{18}$$

$$\hat{H}_B(z) = z^{-1}\hat{H}_{0,B}(z) = \frac{0.008073z + 0.6741}{z^3 - 0.5762z^2 - 0.08815z}. \tag{19}$$

3.2.1 Measured vs simulated response and model error

Only the results concerning motor A are shown considering redundancy. Figure 2 shows the measured angular velocity compared with the simulated responses for both models, zoomed to clearly reveal differences during transient periods. Figure 3 displays the error (difference) between measurement and simulation for each model.

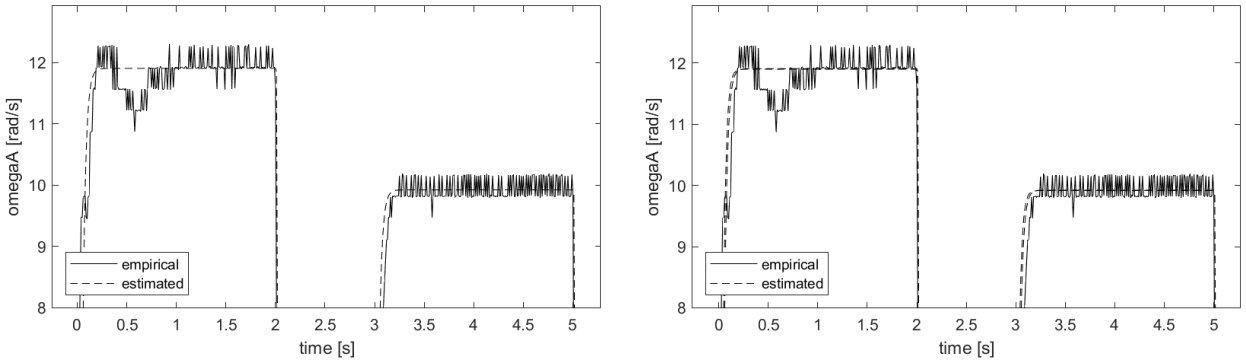

Figure 2: Measured vs simulated responses (left: third-order; right: simplified). Zoomed-in to highlight differences.

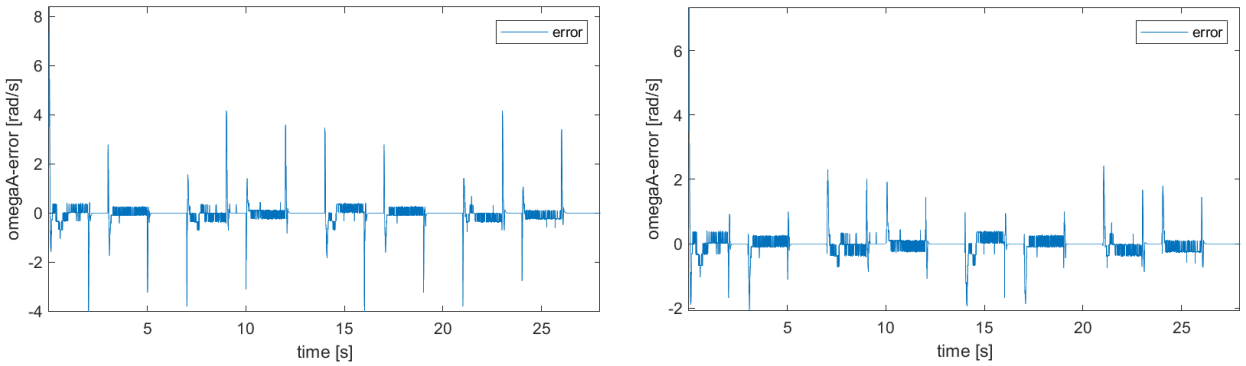

Figure 3: Prediction error (measurement minus simulation). Left: third-order model; right: simplified model.

RMS error (motor A, full model): 0.3611 rad/s
RMS error (motor B, full model): 0.3644 rad/s
RMS error (motor A, simplified model): 0.3723 rad/s
RMS error (motor B, simplified model): 0.3758 rad/s

3.2.2 Transient and steady-state characteristics

Transient behavior: Both models reproduce the measured step-to-step evolution of the angular velocity. The third-order model responds a fraction faster after each voltage transition because the additional pole associated with armature inductance gives a steeper initial slope. The velocity measurements are quantized, so visible level-to-level toggling appears that the continuous models cannot mirror. That discrepancy excites the lightly damped high-frequency mode of the third-order fit and inflates its residuals. With the updated identification, the third-order model attains RMS prediction errors of 0.3611 rad/s for motor A and 0.3644 rad/s for motor B—only marginally below the simplified model's 0.3723 rad/s (motor A) and 0.3758 rad/s (motor B) while requiring more parameters.

Steady-state behavior: Both simulations settle to the measured steady-state angular velocities within the sensor resolution. The apparent steady-state ripple arises from the same quantization and is absent in the simulated trajectories, yet the mean levels match within negligible error.

Armature inductance therefore has no discernible influence on steady-state gain, and the simplified second-order model is selected for subsequent analysis.

3.3 Verification of data filtering to improve identification

3.3.1 Motivation for filtering

Pre-filtering measured signals before parameter estimation is a standard technique to suppress high-frequency measurement noise that corrupts the least-squares regression. In principle, applying a low-pass filter to both input and output preserves the frequency-domain ratio $\hat{H}(e^{j\omega})$ while attenuating noise components above the system bandwidth, thereby reducing parameter variance and improving model fidelity.

We filter both signals:

- Input voltage $v[k]$
- Output angular velocity $\omega_A[k]$ (and $\omega_B[k]$ for motor B)

Filtering only the output would distort the input-output frequency response, biasing the identified transfer function. Filtering both with the same linear-phase filter maintains the correct phase relationship and gain ratio at all frequencies below the cutoff.

3.3.2 Filter design

A sixth-order Butterworth low-pass filter was selected for its maximally flat passband magnitude response and straightforward design. The cutoff frequency was chosen empirically by examining the frequency content of the measurement noise visible in Figures 2 and 3. High-frequency oscillations in the prediction error suggest noise components well above the dominant system pole frequency (approximately 10–15 Hz for the motor dynamics).

Filter characteristics:

- **Type:** Butterworth low-pass filter
- **Order:** 8
- **Cutoff frequency:** 35 Hz (selected to suppress encoder-induced chatter while preserving the dominant dynamics)
- **Implementation:** Zero-phase filtering using `filtfilt` to eliminate phase distortion

The 35 Hz cutoff attenuates the high-frequency ripple observed in the prediction error while keeping the dynamic range of interest intact. Higher cutoffs offered less noise suppression, whereas more aggressive settings below 30 Hz began to erode the transient content needed for accurate identification.

3.3.3 Re-identification with filtered data

After applying the Butterworth filter to both input and output signals using `filtfilt`, the linear least-squares estimation was repeated. The estimated parameter vectors for the third-order model with filtered data are

$$\hat{\boldsymbol{\theta}}_A^{\text{filt}} = \begin{bmatrix} -0.7993 \\ 0.0923 \\ -0.0127 \\ 0.5937 \end{bmatrix}, \quad \hat{\boldsymbol{\theta}}_B^{\text{filt}} = \begin{bmatrix} -0.8033 \\ 0.0941 \\ 0.0132 \\ 0.5773 \end{bmatrix}. \tag{20}$$

These coefficients yield discrete-time transfer functions of the form

$$\hat{H}_{\text{filt}}(z) = \frac{\hat{b}_1 z + \hat{b}_2}{z^3 + \hat{a}_1 z^2 + \hat{a}_2 z}. \tag{21}$$

Re-identifying the simplified second-order model on the filtered data gives

$$\hat{\boldsymbol{\theta}}_A^{\text{simp,filt}} = \begin{bmatrix} -0.6873 \\ 0.6204 \end{bmatrix}, \qquad \hat{\boldsymbol{\theta}}_B^{\text{simp,filt}} = \begin{bmatrix} -0.6875 \\ 0.6351 \end{bmatrix}, \tag{22}$$

with corresponding transfer functions

$$\hat{H}_A^{\text{simp,filt}}(z) = \frac{0.6204}{z^2 - 0.6873z}, \qquad \hat{H}_B^{\text{simp,filt}}(z) = \frac{0.6351}{z^2 - 0.6875z}. \tag{23}$$

Figure 11 (Appendix B) compares the measured angular velocity with the simulated response of the filtered-data model. The continuous-time pole locations, damping ratios, natural frequencies, and step-response characteristics (overshoot, peak time, steady-state gain) are computed via Tustin transformation and the `damp` function, as in the unfiltered case.

The explicit transfer functions (without the microOS delay) are

$$\hat{H}_{0,A}^{\text{filt}}(z) = \frac{-0.01271z + 0.5937}{z^2 - 0.7993z + 0.09234}, \tag{24}$$

$$\hat{H}_{0,B}^{\text{filt}}(z) = \frac{0.01315z + 0.5773}{z^2 - 0.8033z + 0.09407}, \tag{25}$$

and reinstating the one-sample delay gives

$$\hat{H}_A^{\text{filt}}(z) = z^{-1}\hat{H}_{0,A}^{\text{filt}}(z) = \frac{-0.01271z + 0.5937}{z^3 - 0.7993z^2 + 0.09234z}, \tag{26}$$

$$\hat{H}_B^{\text{filt}}(z) = z^{-1}\hat{H}_{0,B}^{\text{filt}}(z) = \frac{0.01315z + 0.5773}{z^3 - 0.8033z^2 + 0.09407z}. \tag{27}$$

3.3.4 Comparison and model selection

RMS prediction error: Direct comparison of RMS errors reveals that filtering does *not* improve identification accuracy. For motor A, the unfiltered third-order model achieves an RMS error of 0.3611 rad/s (0.3644 rad/s for motor B), whereas the filtered third-order fits rise to 0.3865 rad/s and 0.3875 rad/s, respectively. This degradation indicates that the 35 Hz filter eliminates informative transients together with the noise.

Interpretation: The lack of improvement suggests that the dominant error source is *not* high-frequency additive noise but rather model mismatch (e.g., unmodeled nonlinearities, quantization effects, or the lightly damped pole artifact from encoder resolution). Because the simplified second-order model already achieves 0.3723 rad/s for motor A with two parameters and outperforms the filtered third-order alternatives, we conclude that the model structure—not the noise level—is the limiting factor.

Model preference: We therefore retain the **unfiltered simplified second-order model** for all subsequent analysis. This choice is motivated by:

1. Superior or comparable RMS prediction performance (0.3723 rad/s for motor A) without the error penalty observed for the filtered third-order models (0.3865/0.3875 rad/s).
2. Simpler structure (two parameters vs. four), reducing overfitting risk.
3. Absence of the spurious high-frequency oscillations that can appear in the higher-order fit due to encoder quantization.

The filtering exercise confirms that the measurement noise is secondary relative to structural mismatch; a parsimonious model on unfiltered data best captures the true system dynamics under the given experimental conditions.

References

Franklin, Powell, E.-N. (2020). *Feedback Control of Dynamic Systems.* Pearson Education Limited.

A Simplified second-order model (armature inductance neglected)

The simplified discrete-time transfer function neglecting armature inductance L_a is:

$$H(z) = \frac{b_1}{z^2 + a_1 z} \tag{28}$$

This model has two parameters (a_1, b_1) compared to four in the full model.

The recursion expression for the simplified model is given in the main text by (8), with the associated regression vector and least-squares criterion (10). For completeness, we retain the matrix formulation below.

Matrix formulation

For N measurements with maximum delay of 2 samples (starting from $k = 3$):

$$\boldsymbol{y} = \begin{bmatrix} \dot{\theta}[3] \\ \dot{\theta}[4] \\ \vdots \\ \dot{\theta}[N] \end{bmatrix}, \quad \boldsymbol{\Phi} = \begin{bmatrix} -\dot{\theta}[2] & v[1] \\ -\dot{\theta}[3] & v[2] \\ \vdots & \vdots \\ -\dot{\theta}[N-1] & v[N-2] \end{bmatrix} \tag{29}$$

The least squares solution is:

$$\hat{\boldsymbol{\theta}}_N^{LS} = [\boldsymbol{\Phi}^T \boldsymbol{\Phi}]^{-1} \boldsymbol{\Phi}^T \boldsymbol{y} = \boldsymbol{\Phi}^+ \boldsymbol{y} \tag{30}$$

B Figures

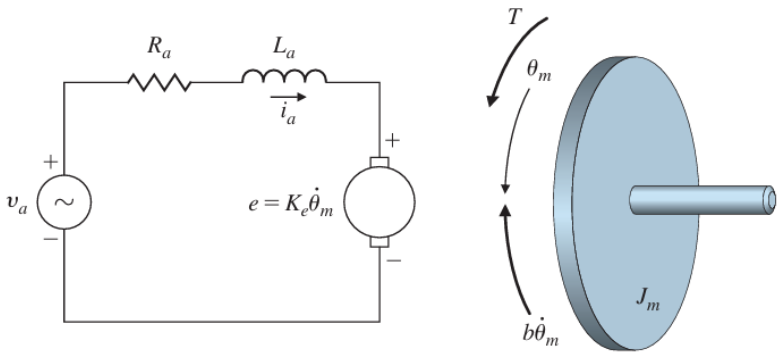

Figure 4: Model of the DC motor Franklin [2020]

Figure 5: Input voltage applied to both DC motors over time

Figure 6: Measured angular velocities for motors A and B

Figure 7: Comparison of signals across periods to assess measurement noise

Figure 8: Model validation without filtering: measured vs simulated response for motor A

Figure 9: Step response of the discrete-time model (unfiltered)

Figure 10: Mean angular velocity for motor A averaged across all measurement periods

Figure 11: Model validation with filtering: measured vs simulated response for motor A

Figure 12: Step response of the discrete-time model (filtered)